Analysis and diagnosis of the composition of ageostrophic circulations in jet-front systems

Jean-Pierre Cammas, Daniel Ramond

Analysis and Diagnosis of the Composition of Ageostrophic Circulations in Jet-Front Systems

JEAN-PIERRE CAMMAS AND DANIEL RAMOND

Observatoire de Physique du Globe de Clermont-Ferrand, Laboratoire de Météorologie Physique, Université Blaise Pascal, Clermont-Ferrand, France

(Manuscript received 23 November 1988, in final form 10 May 1989)

ABSTRACT

Diagnostic case studies of ageostrophic circulations in upper-tropospheric jet–front systems are presented, using the numerical analyses of the ECMWF model as data sources. The impact of the ECMWF analysis procedure on the retrieved ageostrophic fields is first discussed. Upper-level fields of the ageostrophic wind and its divergence are computed in the natural coordinates system in order to analyze the composition of the transverse (cross-stream) and the alongstream ageostrophic components that are induced by alongstream wind variations and curvature effects respectively. The analysis shows that the curvature effects can contribute in a predominant way to the upper-tropospheric divergence field in entrance or exit regions of jet streaks, so as to sometimes inhibit the expected transverse circulations. Several transverse indirect circulations are displayed in the exit regions of jet streaks. A case of lateral shift towards the anticyclonic side of the jet axis of an indirect circulation is discussed with respect to the conceptual approach based on the frontogenetic forcing in highly idealized two-dimensional flow configurations.

1. Introduction

The transverse vertical circulations associated with upper-tropospheric straight jet streaks were first investigated by Namias and Clapp (1949), and subsequently by Bjerknes (1951), Riehl et al. (1952), Murray and Daniels (1953), Reiter (1961) and Cahir (1971). Bjerknes (1951) and Uccellini and Johnson (1979) define the jet-streak circulation patterns as adjustments of the mass field to the momentum field at synoptic to mesoscales. Alongstream wind variations in the entrance and the exit region of a straight jet streak induce transverse (cross-stream) ageostrophic motions, which involve mass adjustments in the depth of the troposphere and then an isallobaric response to these adjustments in the lower troposphere. Figure 1a shows the deduced patterns of two-dimensional direct and indirect vertical circulations respectively in entrance and exit regions of straight jet streaks. Reiter (1969), Danielsen (1974), Uccellini and Johnson (1979), Blustein and Thomas (1984), Brill et al. (1985), Uccellini et al. (1984, 1987), and Achtor and Horn (1986) have related the effects of these vertical circulations to the cyclogenesis and to the development of severe convection for several case studies. Uccellini and Johnson (1979) investigated the role of transverse circulations in the coupling of upper-level jet streaks and low-level jets and surface fronts.

In view of an analysis of the frontogenetical processes leading to the formation and to the maintenance of upper-level frontal zones associated with straight jet streaks, Shapiro (1981, 1982, 1983), Keyser and Pecnick (1985a,b), and Keyser and Shapiro (1986) investigated the interplay between geostrophic and transverse ageostrophic circulations within jet–front systems. In order to explain the observed vertical circulation in jet–front systems Shapiro (1981) argues that, in case of highly idealized two-dimensional flow configuration involving a straight jet–front system, a suitable approximation is the geostrophic momentum approximation introduced first by Eliassen (1948). By qualitative deductions from the Sawyer–Eliassen diagnostic equation (Sawyer 1956; Eliassen 1962), Shapiro (1981, 1983) and Keyser and Shapiro (1986) consider the combined effects of confluence (diffluence) and horizontal shear in forcing direct (indirect) vertical transverse circulations in the entrance (exit) region of a jet streak. Shapiro (1981, 1983) argues that the thermal advection observed in an evolving baroclinic wave, a consequence of the phase difference between the geopotential height and thermal waves, provides the ageostrophic circulations the possibility to be forced by both confluence (diffluence) and horizontal shear. Keyser and Shapiro (1986) derived from the Sawyer–Eliassen equation that, in absence of horizontal shear, direct and indirect vertical circulations in the

Corresponding author address: Dr. Daniel Ramond, Laboratoire de Météorologie Physique, Université Blaise Pascal, 63000 Clermont-Ferrand, France.

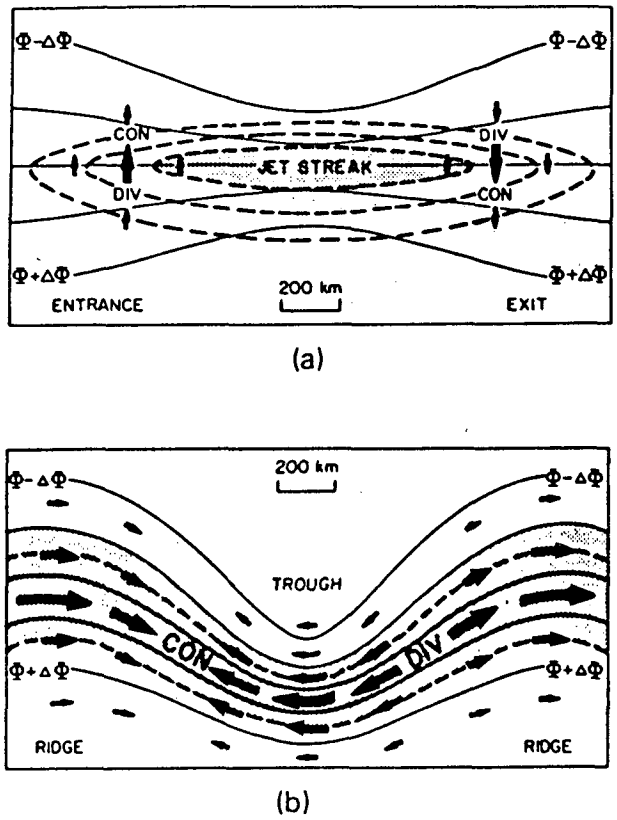

FIG. 1. Schematic representation of the ageostrophic motions (heavy arrows) and associated patterns of convergence (CON) and divergence (DIV) in the vicinity of (a) a straight jet streak in the absence of along-contour thermal advection (after Bjerknes 1951) (b) a uniform jet stream within a stationary synoptic scale wave (after Bjerknes and Holmboe 1944). Both representations are assumed to apply at or near the level of maximum wind, where the horizontal wind distribution is most distinct and the flow is approximatively horizontal. Solid lines indicate geopotential height on a constant pressure surface; dashed lines are isotachs (maximum wind speed dashed). Adapted from Shapiro and Kennedy (1981).

confluent entrance and diffluent exit regions, respectively, are centered about the jet axis, as shown by Fig. 1a. In cases of upper-tropospheric thermal advection resulting from horizontal shear, the predicted effect of the superimposed horizontal shear is to shift the direct and indirect circulations laterally towards the cyclonic or anticyclonic side of the jet axis, depending on the sign of the thermal advection.

However attractive the concepts of ageostrophic circulations developed from the Sawyer–Eliassen equation may be, we must bear in mind the limitations of this equation. Based on the geostrophic momentum approximation and the thermal wind relation, the diagnostic equation describes only the ageostrophic circulations that are required to tend back towards a geostrophic balance. By neglecting the effects of the advection and of the temporal variations of the ageostrophic component of the wind, the Sawyer–Eliassen ageostrophic circulations do not take into account the contributions of the nongeostrophic processes which make that the atmosphere do not always tend towards a geostrophic balance (Uccellini et al. 1984). Furthermore, the application of the geostrophic momentum approximation on a straight frontal zone, i.e., the cross-front geostrophy approximation, implicitly states that it is the wind field that adjusts to the thermal field which is not initially the case for synoptic to mesoscales. The deductions from the Sawyer–Eliassen equation should be used to make easier the understanding of the role of ageostrophic circulations on upper-level frontogenesis for idealized flows situations.

The numerical results obtained by Keyser and Pecnick (1985a,b), with a two-dimensional primitive equation model of frontogenesis applying to idealized two-dimensional flow pattern, are in agreement with the qualitative deductions described above. In a cold advection case, they illustrate the shift of the direct circulation on the anticyclonic side of the jet axis and the frontogenetical effect of such a circulation coming from a strong midtropospheric subsidence beneath the jet core on the warm side of the developing baroclinic frontal zone. As observed in experimental case studies (Staley 1960; Danielsen 1968; Reiter 1975; Shapiro 1980; Uccellini et al. 1985; Uccellini 1986), strong midtropospheric subsident velocities on the warm side of the frontal zone are associated with a tropopause fold event, a process by which air originating from the lower stratosphere penetrates deeply into the midtroposphere, sometimes reaching the 700 mb level (Danielsen 1959).

Beebe and Bates (1955) have first studied the issue of centripetal acceleration induced by significant curvature in the flow with respect to the straight jet streak circulation pattern. Buzzi et al. (1977), Shapiro (1981), Newton and Trevisan (1984a,b), Uccellini et al. (1984) and Keyser and Shapiro (1986) examine the three-dimensional modifications, introduced by curvature in the flow, to the two-dimensional vertical circulation patterns considered above. Results of simulation of a baroclinic wave growth with the three-dimensional β-plane channel model of Newton and Trevisan (1984a,b), in the absence of transverse ageostrophic circulations, show the frontogenetical influence of an along-contour (geopotential contour) ageostrophic component induced by curvature of the flow. Accordingly to Bjerknes and Holmboe (1944), Keyser and Shapiro (1986) proposed, in a case of a uniform jet stream within a stationary synoptic scale wave, a schematical representation of the divergence field (Fig. 1b) based on the gradient flow concept. Upstream of the trough the subsidence related to along-contour variations in curvature is shown to be frontogenetical for parcels migrating from the upstream ridge to the base of the trough, and is favorable for a tropopause fold event (Newton and Trevisan 1984a,b).

Following their conceptual approach, Keyser and Shapiro (1986) conclude that in the case of a jet–front

system located at the base of a long-wave trough, the effect of curvature is to reinforce the vertical branches of the transverse ageostrophic circulations beneath the jet axis. Such a conceptual approach is of considerable interest as it simplifies the understanding of the dynamical processes which produce vertical circulations in upper-level frontal zones. However, because of the gaps in observational data (spatial coverage and temporal resolution), additional case studies are recommended to examine the relative contributions of the transverse and alongstream components of the ageostrophic circulations to upper-level frontogenesis, during the life cycle of baroclinic waves.

Such is the purpose of the present study in which we present, for several experimental situations, diagnostic analyses of ageostrophic circulations in jet–front systems. We have used the numerical analyses of the European Centre for Medium-Range Weather Forecasts (ECMWF) model as data sources, taking advantage of the regular latitude–longitude gridded form, the dynamical consistency and the spatial coverage of these datasets to work in natural coordinates. With a simple method, fields of cross- and alongstream components of the ageostrophic wind, that are associated with alongstream speed changes and centripetal accelerations respectively, are displayed. Their relative contributions to the upper-level divergence field are analyzed in order to diagnose ageostrophic circulations in the entire depth of the troposphere.

Section 2 is a description of the ECMWF analysis scheme valid for 1984 in order to measure the potential impacts of such an assimilation scheme on our results. In sections 3 and 4, diagnosis and analysis of the transverse and the alongstream ageostrophic components are made for two case studies. Section 5 presents the analysis of a case of warm advection. Results are summarized in section 6.

2. A brief description of the ECMWF analysis scheme

The analyzed variables are geopotential height and wind components at 15 standard pressure levels from 1000 to 10 mb, and geopotential thickness between them. A regular 1.875° latitude–longitude grid is used. The data assimilation scheme includes a numerical model which can update the information from past observations to the current analysis time, and an assimilation of all the data with a fully three-dimensional optimum interpolation method, multivariate in wind, height and thickness (Lorenc 1981; Lonnberg and Shaw 1986). Observed minus first-guess (the 6 hour forecast) deviations for all the variables are analyzed to give increment fields which are then added to the forecast fields. The geopotential height errors and their correlations are first statistically specified as a smooth global three-dimensional field. Wind errors and their correlations are derived by modeling the streamfunction and velocity potential errors. The velocity potential errors are assumed to be negligible, which constrain the analyzed wind increments to be nondivergent. For multivariate height and wind analyses, the cross-correlations between height (and hence thickness) and wind errors are specified assuming that the height and wind covariance errors obey the geostrophic relationship. Then the analyzed increments would do so also. The hydrostatic relationship enters in the conversion of temperature observations to thicknesses. The analyzed vertical velocities are obtained from the computation of the horizontal divergence in the equation of continuity.

As described above the nondivergence and the geostrophic relationships of the analyzed increments are the only constraints in the ECMWF analysis scheme. Then the divergence and the ageostrophic wind in the analysis field come principally from the forecast model, that is to say, from the primitive equations. Since no other hypothesis or constraint—such as the gradient wind balance for example—is added, there is no particular biases or forcings towards either of the components of the ageostrophic wind that are associated with alongstream speed changes or centripetal accelerations in the flow. In order to complete the issue about an eventual impact of the analysis procedure on the computed ageostrophic wind fields, we have verified on a few examples (not shown) that for the same absolute time the ageostrophic winds derived from the analysis and from the 6 hour forecast fields are nearly identical. It is thus concluded that there is no noteworthy bias imposed by the analysis procedure on the computed ageostrophic wind fields.

The analysis fields used in this study are the uninitialized fields; they usually fit the individual observations somewhat better than the initialized fields filtered by a projection on normal modes deduced from the primitive equations. Relative to the horizontal ageostrophic wind field it amounts to the same thing to use the initialized or uninitialized fields because the normal modes of the forecast model are compatible with the first-guess wind and therefore compatible with the ageostrophic wind in the first-guess field. The analyzed vertical velocities are less smoothed in the uninitialized fields than in the initialized fields, but there is no disadvantage to use them according to the characteristic scales of our study.

We have used a 1.5° latitude–longitude grid which should be regarded as a practical lower limit for the bilinear interpolation of the analyzed upper fields due to the triangular truncation scheme used at ECMWF (Meteorological Bulletin of ECMWF, 1982). The smoothing of the fields is that linked to the analysis scheme; i.e., (i) the 1.875° analysis grid, (ii) the resolutions of the observations, (iii) the resolution of the correlation functions of the optimal interpolation (a T35 scheme in 1984; i.e., a 300 to 400 km resolution). Although it is difficult to define the resolution of the analysis field—due to a large variance of the resolution

of the observations—an average resolution of 200 to 400 km would be accounted.

It is clear that the vertical resolution in the analyzed fields is a constraint that may tend to eliminate interesting features for our use, such as tropopause folds. The studies of Elsberry and Kirchoffer (1988) have demonstrated how much detail is lost making use of the ECMWF analysis data on the mandatory levels for cross sections in tropopause fold, as compared to the same cross sections using available radiosonde data in the studies of Uccellini et al. (1985). However, at jet-stream level the scale of the regular latitude–longitude gridded data of the ECMWF analysis fields is compatible with the spatial variations of speed along the axis of the jet stream, and with the scales of associated dynamical features in the wind relevant to our study. In order to present the results we have selected the 300 mb level for all the horizontal analyses pertaining to the upper-troposphere. Indeed, at this level the jet pattern is well defined, particularly for real and ageostrophic wind fields and for divergence fields. The frontal gradients in the temperature fields at this level are typically more diffuse than those at a lower level (about 400 mb), however the separation of phases between height and thermal waves and the so-called different cases of cold or warm advection can be distinguished at this level.

3. Case study: 1 June 1984 at 1800 UTC

a. Synoptic situation

Figure 2a shows the geopotential and temperature fields in the upper troposphere on 1 June 1984 at 1800 UTC over western Europe. The geopotential wave is characterized by a meridionally oriented trough, the axis of which is noted T on Fig. 2a about 15°W, and a ridge R oriented southwest to northeast about 10°E. At 1800 UTC 1 June 1984 two jet streaks, noted JS1 and JS2, respectively, on Fig. 2b, are diagnosed upstream and downstream of T. This general spatial pattern is maintained during the baroclinic wave evolution between 1 and 3 June 1984; the trough axis reaches 5°W by 0600 UTC on 3 June 1984, as can be seen on Fig. 19. In order to get an additional sense of the adequacy of the ECMWF analyses for the present purposes we have also displayed on Fig. 3 the radiosonde data at 300 mb for one synoptic time analysis at the beginning of the case study, at 1200 UTC 2 June 1984.

b. Ageostrophic wind field in the upper troposphere

We define a natural coordinate system where s is the alongstream (longitudinal) coordinate parallel to the wind vector **V** and n is the cross-stream (transverse) coordinate perpendicular and to the left of the horizontal flow (see Fig. 4), as it has been used by Uccellini and Johnson (1979), Shapiro and Kennedy (1981) and Achtor and Horn (1986). In this natural coordinate system the frictionless form of the horizontal equation of motion is:

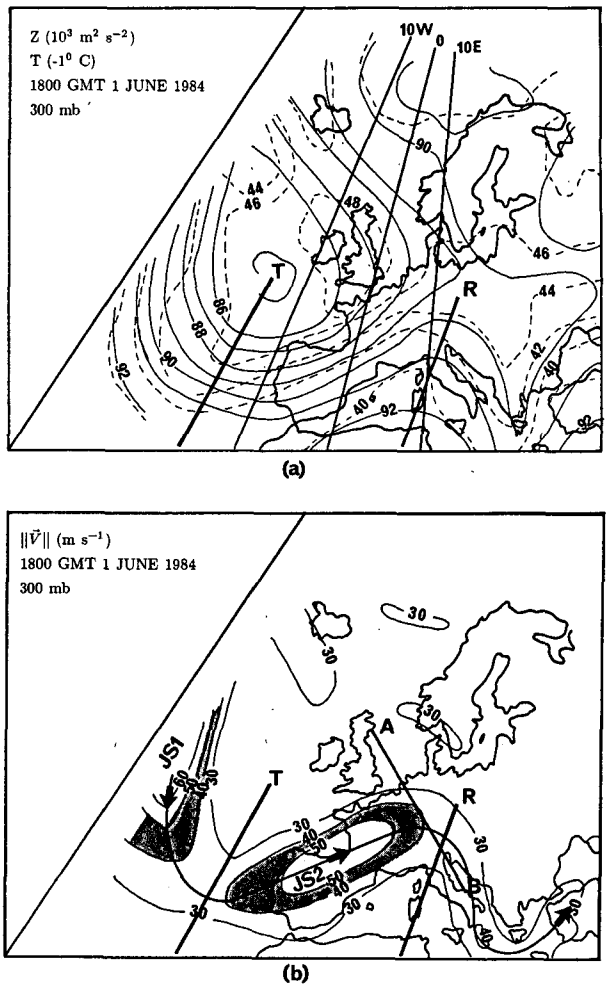

FIG. 2. (a) Geopotential and temperature fields at 300 mb for 1800 UTC 1 June 1984, geopotential contours are drawn in solid lines ($\times 10^3$ m^2 s^{-2}), isotherms in dashed lines (°C). The trough and ridge axes are noted T and R, respectively. The meridians 10°W, 0°, and 10°E are displayed. (b) 300 mb wind field for 1800 UTC 1 June 1984, isotachs in m s^{-1} for speed greater than 30 m s^{-1}, shading represents wind speed interval between 40 and 50 m s^{-1} to depict jet streaks indicated by JS1 and JS2. The line with arrows indicates the axis of highest wind speeds. AB indicates the plane of the cross section of Fig. 11.

$$V_{an} = +f^{-1}\frac{dV}{dt} \tag{1}$$

$$V_{as} = -f^{-1}\frac{V^2}{R_t} \tag{2}$$

where V_{an} is the ageostrophic wind component transverse to the flow, V_{as} is the alongstream ageostrophic component, V is the wind velocity, f is the Coriolis parameter, and R_t is the curvature radius of the trajectory. The ageostrophic component V_{an} is associated

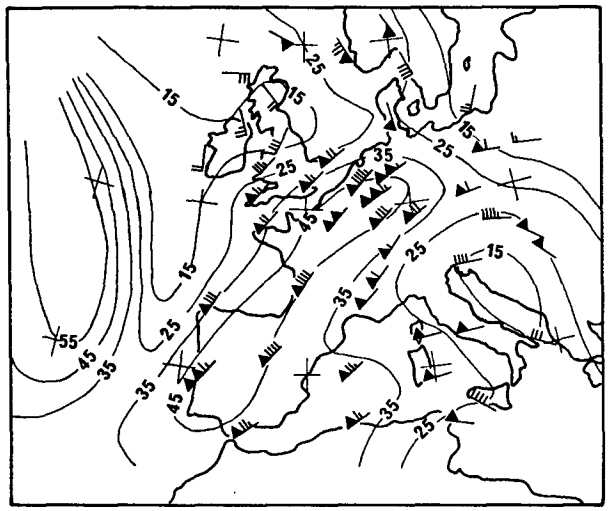

FIG. 3. Wind field at 300 mb for 0000 UTC 2 June 1984, isotachs in m s^{-1} every 10 m s^{-1} (ECMWF analysis data). Radiosonde winds at 300 mb for synoptic stations, each flag denotes 25 m s^{-1}, each full barb denotes 5 m s^{-1}, each half-barb denotes 2.5 m s^{-1}. Crosses every 10° in latitude and longitude.

with alongstream speed changes, while the component V_{as} is associated with the centripetal acceleration on a curved trajectory.

Figure 5a shows the transverse ageostrophic component V_{an} field computed by vectorially subtracting the geostrophic wind from the analyzed wind, and by projecting ageostrophic wind vectors in the natural coordinate system defined by the analyzed wind vectors. Ageostrophic transverse flow towards greater heights of the order of −15 and −10 m s^{-1} is shown in the exit

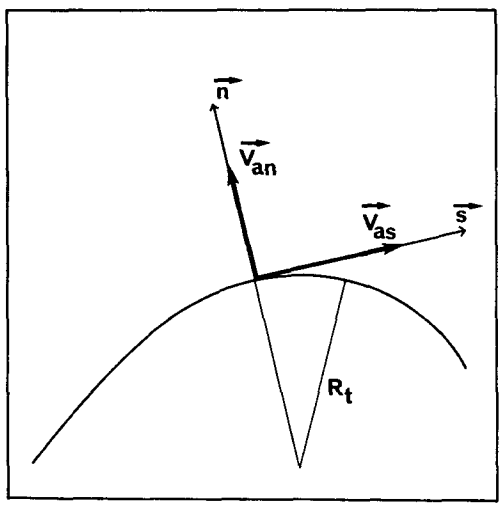

FIG. 4. Schematic of the natural coordinate system used. Streamline (solid curve) of the flow with the two components $\mathbf{V}_{an}$ and $\mathbf{V}_{as}$ of the ageostrophic wind along the natural vectors $\mathbf{n}$ and $\mathbf{s}$, R_t radius-of-trajectory curvature for a finite element of the streamline.

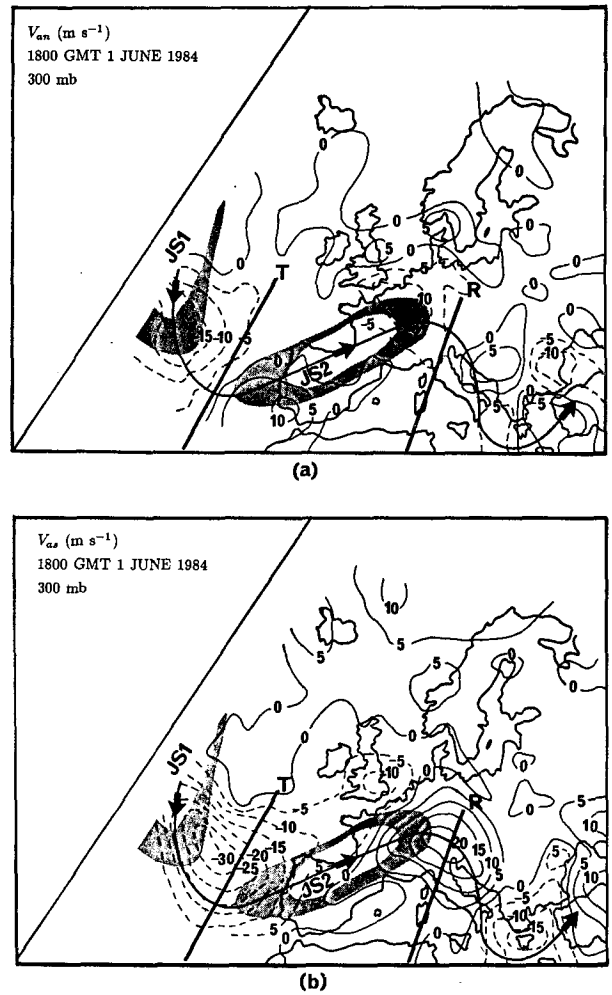

FIG. 5. (a) Transverse ageostrophic wind component V_{an} at 300 mb for 1800 UTC 1 June 1984. Positive values in solid lines, negative values in dashed lines, units in m s^{-1}. Key features as in Fig. 2b. (b) Alongstream ageostrophic component V_{as} at 300 mb for 1800 UTC 1 June 1984. Positive values in solid lines, negative values in dashed lines, units in m s^{-1}. Key features as in Fig. 2b.

regions of jet-streaks JS1 and JS2, respectively. The ageostrophic transverse flow V_{an} towards lower heights reaches the maximum values of the order of +10 m s^{-1} in the entrance region of the jet streak JS2; this maximum of V_{an} is not centered about the jet axis, but is shifted laterally on its anticyclonic side. This last observation will be discussed in section 5.

Figure 5b shows the alongstream ageostrophic component V_{as} field in the upper troposphere. Strong negative and positive values of V_{as} of the order of −30 and +20 m s^{-1} are found near the trough T and ridge R axes, respectively. The values of V_{an} and V_{as} displayed on Figs. 5a and 5b are in good agreement with those obtained by Achtor and Horn (1986) although the method used is quite different. These authors used the horizontal vector equation of motion in natural co-

ordinates to compute on a 2° × 2° grid the cross- and alongstream components of the ageostrophic wind, assuming that at the level 300 mb the primary contributions are the curvature and speed-advection.

As can be seen by comparing V_{an} to V_{as} fields (Figs. 5a and 5b), most of the ageostrophic wind in the exit and entrance regions of the jet streaks JS1 and JS2 respectively is due to curvature. Therefore, concerning the total ageostrophic wind field we find that contributions due to centripetal acceleration associated with cyclonically or anticyclonically curved trajectories can be also predominant in the entrance or the exit regions of jet streaks. The flow pattern in the present case study, with a jet streak embedded between a trough and a ridge axis, is a complementary case study of those integrated in the idealized scheme of the progression of the jet–front system in a baroclinic wave that has been reviewed by Keyser and Shapiro (1986, see their Fig. 19). In the conceptual model derived by these authors the curvature effects are taken into account when the jet–front system is at the base of the long-wave trough, a flow pattern in which the flow curvature is relatively weak in the entrance and the exit region of the jet streak, and is significant at its center.

In order to establish a diagnostic of ageostrophic circulations in the depth of the troposphere we now examine the divergence field in the upper troposphere, concentrating on fields at the 300 mb level.

c. *Divergence fields in the upper troposphere*

1) Divergence field of the ageostrophic wind

On a constant pressure surface, the ageostrophic divergence is expressed as:

$$\nabla_p \cdot \mathbf{V}_a = \nabla_p \cdot \mathbf{V} - \nabla_p \cdot \mathbf{V}_g \qquad (3)$$

with

$$\nabla_p \cdot \mathbf{V}_g = \frac{-v_g}{R_T} \cot g\phi \qquad (4)$$

where v_g is the meridional geostrophic wind component, R_T is the radius of earth and ϕ is the latitude. Both total divergence and ageostrophic divergence maxima are of the order of 4 to 5 ($\times 10^{-5}$ s^{-1}) in our case study, whereas geostrophic divergence maxima are of the order of 0.6×10^{-5} s^{-1}. So, we examine the divergence field of the ageostrophic wind to interpret the divergence and convergence maxima of the total wind field, neglecting in a first approximation the geostrophic divergence.

Figure 6 displays the divergence field of the ageostrophic wind in the upper troposphere at 1800 UTC 1 June 1984. For clarity, the convergence and divergence maxima are noted as follows:

- C1 for the convergence maximum upstream the trough axis T,

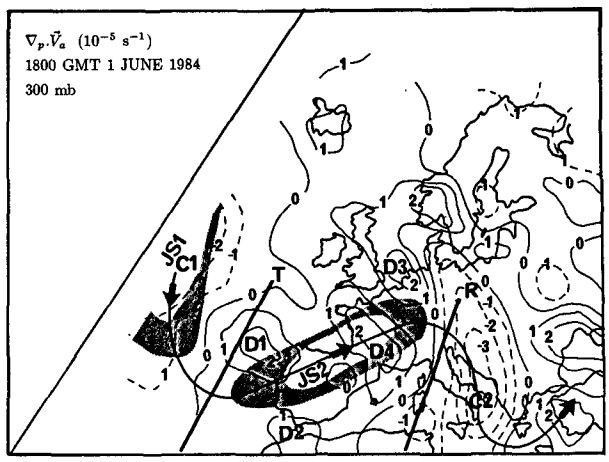

FIG. 6. Ageostrophic divergence field at 300 mb for 1800 UTC 1 June 1984; positive values in solid lines, negative values in dashed lines, units ($\times 10^{-5}$ s^{-1}). Key features as in Fig. 2b.

- D1 and D4 for the two divergence maxima between the trough T and ridge R axes,
- D2 for the divergence maximum on the anticyclonic side in the entrance region of the jet streak JS2,
- D3 for the divergence maximum on the cyclonic side in the exit region of the jet streak JS2,
- C2 for the convergence maximum downstream of the ridge axis R.

2) Contributions of the natural components of the ageostrophic wind

In order to investigate the contributions of both the transverse and longitudinal ageostrophic wind components to each maximum in the upper-level divergence field, we compute the ageostrophic divergence in the natural coordinate system as

$$\nabla_p \cdot \mathbf{V}_a = \frac{\partial V_{an}}{\partial n} + \left[\frac{\partial V_{as}}{\partial s} + \frac{V_{an}}{R_t} - V_{as}\frac{\partial \psi}{\partial n}\right] \qquad (5)$$

where ψ is the wind direction in the meteorological convention. If the air travels much more rapidly than the streamline patterns, which is usually the case, one may with some approximation (Reiter 1961) equalize the trajectory curvature $K_t = 1/R_t$ and the streamline curvature defined by

$$K_s = \frac{1}{R_s} = \frac{\partial \psi}{\partial s}. \qquad (6)$$

In a case of a negligible curvature of the flow, the bracketed terms of the Eq. (5) tend to zero. They total the contribution of the curvature of the flow to the ageostrophic divergence, whereas the term $\partial V_{an}/\partial n$ of this equation is the contribution of the alongstream speed changes in a straight flow.

For the convenience of our purpose the Eq. (5) can be also written:

$$\nabla_p \cdot \mathbf{V}_a = \mathrm{T1} + [\mathrm{T2} + \mathrm{T3} + \mathrm{T4}]$$
$$= \mathrm{T1} + [\mathrm{T2} + \mathrm{T34}] = \mathrm{T1} + [\mathrm{T234}] \quad (7)$$

where all the bracketed terms are curvature terms.

Gradients in the natural coordinate system are defined through the following operators:

$$\frac{\partial}{\partial s} = \mathbf{s}\cdot\nabla = \frac{1}{\|\mathbf{V}\|}\mathbf{V}\cdot\nabla = \frac{1}{\|\mathbf{V}\|}\left(u\frac{\partial}{\partial x} + v\frac{\partial}{\partial y}\right) \quad (8)$$

$$\frac{\partial}{\partial n} = \mathbf{n}\cdot\nabla = \frac{1}{\|\mathbf{V}\|}\nabla\cdot(\mathbf{k}\wedge\mathbf{V})$$
$$= \frac{1}{\|\mathbf{V}\|}\left(-v\frac{\partial}{\partial x} + u\frac{\partial}{\partial y}\right) \quad (9)$$

where x and y are the coordinates in the Cartesian system oriented west–east and south–north, respectively, and u and v are the zonal and the meridional components of the wind respectively.

The computation of the ageostrophic divergence in the natural coordinate system with Eq. (5) implicitly depends on the determination of the radius of trajectory curvature, whereas the one performed in the Cartesian coordinate system with Eq. (3) does not. So, the use of the natural coordinate system, with a resolution defined on the 1.5° gridded dataset of ECMWF analyses, in regions of lowest speed flow and strong gradients in curvature, should be viewed with some caution. We exclude from the further interpretations of the divergence field the stippled regions displayed on Fig. 7 because of the lack of precision obtained in computing the ageostrophic divergence in the natural coordinate system. In these last regions the absolute difference E between ageostrophic divergences computed with Eqs. (3) and (5), respectively, i.e.:

$$E = \left|(\nabla_p\cdot\mathbf{V} - \nabla_p\cdot\mathbf{V}_g) - \left(\frac{\partial V_{an}}{\partial n} + \left[\frac{\partial V_{as}}{\partial s} + \frac{V_{an}}{R_t} - V_{as}\frac{\partial\psi}{\partial n}\right]\right)\right| \quad (10)$$

is more than 0.3×10^{-5} s^{-1}, about 10% of the maximum divergence field observed. As can be seen on the ageostrophic divergence field computed through Eq. (3) and displayed on Fig. 6, there is no ageostrophic divergence (convergence) maximum in the stippled regions displayed on Fig. 7. So, the lack of precision obtained in computing ageostrophic divergence wind field in the natural coordinate system is not a limitation for our purpose.

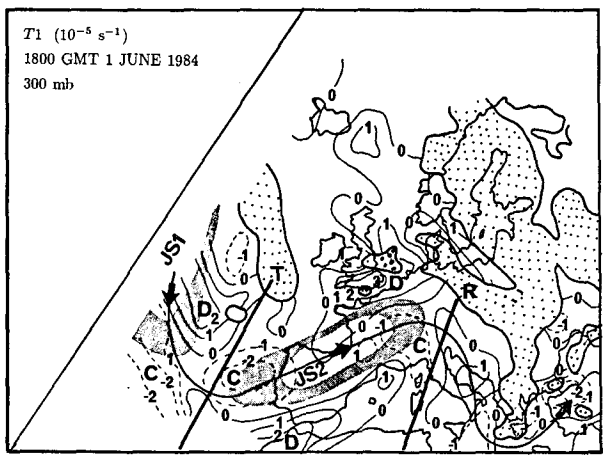

FIG. 7. Ageostrophic divergence field related to the term T1 (see text) at 300 mb for 1800 UTC 1 June 1984, positive values in solid lines, negative values in dashed lines, units ($\times10^{-5}$ s^{-1}). Stippled regions are regions for which the quantity E (see text) is greater than 0.3×10^{-5} s^{-1}. Key features as in Fig. 2b.

(i) *The transverse ageostrophic wind component V_{an}*

Figure 7 displays the contribution to the ageostrophic wind divergence field of the term $\partial V_{an}/\partial n$ in (5), i.e., the term T1. This field would be the divergence induced by the transverse ageostrophic wind component, in the case of negligible curvature of the flow. As expected this field schematically reproduces the "four-cell" pattern of convergence and divergence in the vicinity of a straight jet streak (Fig. 1a), as they can be deduced from considerations about the alongstream wind speed variations (Bjerknes 1951; Uccellini and Johnson 1979). The centers of convergence and divergence in the entrance and the exit regions of the jet streak JS2 and those in the exit region of the jet streak JS1 are indications of the direct and the indirect circulations related to the jet streak JS2, and of the indirect circulation in the exit region of the jet streak JS1 respectively. In the entrance region of the jet streak JS2, the lateral shift, towards the anticyclonic side of the jet axis, of the convergence and divergence centers is in agreement with Shapiro's deductions (1981) on the effect of the horizontal shear in case of alongfront thermal advections, and will be discussed in section 5.

However, the comparison between Figs. 6 and 7 shows that the contribution of the term $\partial V_{an}/\partial n$ to the ageostrophic divergence is not predominant, only the divergence maxima D2 and D3 result from the contribution of this last term. Thus, the signatures of both direct and indirect transverse circulations observed in the $\partial V_{an}/\partial n$ field (Fig. 7) relative to the jet streaks JS1 and JS2 are only partially reproduced in the total ageostrophic divergence field (Fig. 6). Therefore significant contribution of the curvature effect to the upper-tropospheric divergence field is evident.

(ii) *The longitudinal ageostrophic wind component V_{as}*

Figure 8 displays the ageostrophic divergence field related to the curvature terms in the Eq. (5); i.e., the term noted T234 [see Eqs. (5) and (7)]. A comparison of Figs. 6, 7 and 8 shows that the curvature terms in

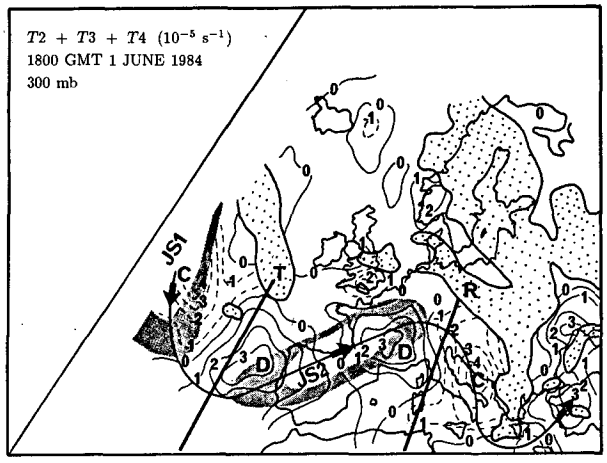

FIG. 8. Ageostrophic divergence field related to the term T234 (see text) at 300 mb for 1800 UTC 1 June 1984, positive values in solid lines, negative values in dashed lines, units ($\times 10^{-5}$ s^{-1}). Key features as in Fig. 2b and Fig. 7.

the Eq. (5) yield a predominant contribution to the total ageostrophic divergence. Thus, the convergence and divergence maxima C1, C2, D1, D4 observed on the total ageostrophic divergence field are the signature of curvature effects, which appears to be predominant in this case study. Uccellini et al. (1984) have discussed the evolution of the upper-level divergence field and associated changes in the transverse circulations when a jet streak approaches a ridge axis. They found that the curvature effects imply a basic contribution to the maximum divergence immediately upstream of the ageostrophic wind maximum near the ridge axis. The location of the divergence maximum D4 (Fig. 6) shows that our results are in good agreement with those of Uccellini et al. (1984).

Furthermore we can see that all the maxima of convergence (divergence) C1, C2 (D1, D4) are located within the strong negative (positive) alongstream gradients of the ageostrophic wind component V_{as} (see Fig. 5b). According to this last observation, the contribution of the two most right bracketed term in (5); i.e., the term T34 to the total ageostrophic divergence appears weak, which is confirmed by the striking similarity of the T234 field (Fig. 8) and the T2 field (Fig. 9). For the flow pattern of this case study (i.e., a jet streak embedded between a trough and a ridge axis) an analysis of the signs of the terms T3 and T4 [see Eqs. (5) and (7)] show that they are opposite on both sides of the trough T or the ridge R axis which explains their weak total contribution. However, the possibility to neglect in a first approximation the contribution of the T34 term to the total divergence, which permits an interpretation of the divergence field with only the fields of the natural components of the ageostrophic wind, should be examined for each case study. In a case of a jet streak at the base of a long-wave trough, an identical analysis of the T3 and T4 signs would show that they are of the same sign as each other on both sides of the trough axis, which does not allow us to neglect their total contribution a priori.

Most of the contribution of curvature terms to the upper-level divergence field in the present case study is induced by alongstream gradients of the component V_{as}. Now, we are comparing this contribution to that deduced with the gradient wind concept.

(iii) *Contributions of the curvature advection term*

Shapiro (1983) and Keyser and Shapiro (1986) have defined an idealized case of pure along-contour ageostrophic flow which satisfies all the assumptions leading to the gradient wind. This case consists in a uniform jet stream within a stationary synoptic-scale wave in which horizontal speed changes dV/dt vanish, eliminating the cross-stream ageostrophic flow (Fig. 1b). The horizontal divergence of the gradient wind, for this idealized case of flow configuration is expressed as

$$\nabla_p \cdot \mathbf{V}_{gr} = -\left(1 + \frac{KV_{gr}}{f}\right)^{-1}\left[\frac{\beta}{f} v_{gr} + \frac{V_{gr}}{f}(\mathbf{V}_{gr} \cdot \nabla_p K)\right]. \tag{11}$$

This expression contains two contributions: (i) a term proportional to the β effect, namely $\beta v_{gr}/f$, where v_{gr} is the meridional component of the gradient wind $\mathbf{V}_{gr}$, and (ii) a term proportional to the advection of curvature weighted by the gradient wind speed, namely $V_{gr}(\mathbf{V}_{gr} \cdot \nabla_p K)/f$. This last term is predominant (Keyser and Shapiro 1986) and induces maximum convergence (divergence) values at the flow inflection upstream (downstream) of the trough axis along the highest wind speeds (Fig. 1b).

In the T2 field (Fig. 9), two maxima of divergence are observed between the trough T and ridge R axis.

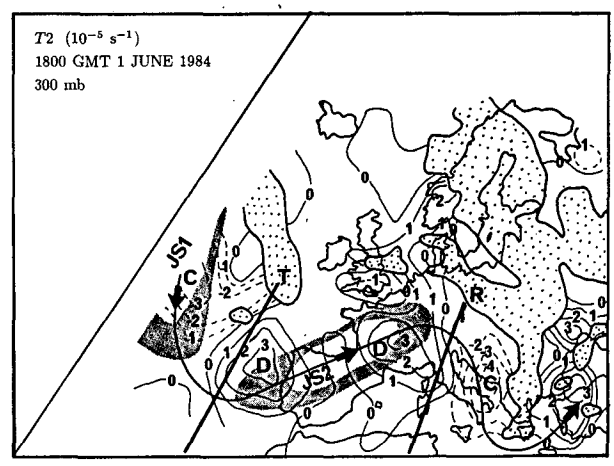

FIG. 9. Ageostrophic divergence field related to the term T2 (see text) at 300 mb for 1800 UTC 1 June 1984, positive values in solid lines, negative values in dashed lines, units ($\times 10^{-5}$ s^{-1}). Key features as in Fig. 2b and Fig. 7.

They correspond to the maxima noted D1 and D4 in the total ageostrophic divergence field (Fig. 6). These two maxima are located in regions of strongest positive alongstream gradients of the component V_{as}, on each side of the flow inflection region which is approximately located nearby the line $V_{as} = 0$. The first maximum D1 immediately downstream of the trough axis T is far from both the flow inflection regions and the high speed regions, which is in opposition to the conclusions suggested by the concept of the gradient wind. Thus, a significant difference is observed with the scheme of Fig. 1b, which furthermore shows only one maximum of divergence between the trough and the ridge axis of the wave. On the other hand, two maxima of convergence, noted C1 and C2, respectively, in the total ageostrophic divergence field, are observed in the T2 field upstream the trough axis T and downstream the ridge axis R. They are located nearby the flow inflection in regions of strongest negative alongstream gradients of the component V_{as}. Their locations are in good agreement with that displayed on the schematic field of the Fig. 1b.

In order to get a closer comparison of the contribution of curvature in the present case study against the one deduced from the gradient flow concept, we have developed the expression of the term T2 to bring out the curvature advection term, the contribution of which is predominant in the horizontal divergence of the gradient wind. If in a first approximation the variation of the Coriolis parameter f is neglected, the term T2 can also be written:

$$\mathrm{T2} = \frac{-1}{f}\left(2VK\frac{\partial V}{\partial s} + V^2\frac{\partial K}{\partial s}\right). \qquad (12)$$

Then the term T2 contains two contributions: (i) a term proportional to the alongstream speed gradient, which does not exist in the aforementioned idealized case of a uniform jet stream within a stationary synoptic-scale wave, and (ii) a term proportional to the advection of curvature weighted by the wind and similar to the one in Eq. (11). A straightforward analysis of the sign of the two right terms of Eq. (12) in the region where the divergence maximum D1 is observed shows that these two terms are of opposite sign, the term of curvature advection being positive and contributing in a predominant way to the formation of the divergence maximum D1. As a matter of fact, in this region downstream of the trough T axis, we have ($K > 0$) and ($\partial K/\partial s \leqslant 0$), and then a positive contribution by the curvature advection term. It is also the entrance region of the jet streak JS2 and we have ($\partial V/\partial s \geqslant 0$), and then a negative contribution by the first right term in Eq. (12). An identical analysis of sign in the regions, where the divergence and convergence maxima D4, C1, C2 are respectively observed, shows the same results: all these maxima are induced by a predominant contribution of the curvature advection term.

We find that the contribution of the curvature advection term to the total ageostrophic divergence field is the predominant contribution induced by curvature effects, as it could be deduced from the gradient wind concept. Nevertheless we find that the locations of the associated convergence and divergence maxima are not necessary in the regions of flow inflection but are in the regions of strongest alongstream gradients of the longitudinal ageostrophic component V_{as}.

An analysis of the composition of cross- and alongstream ageostrophic components can now be made and allows us to discuss three-dimensional modifications introduced by curvature effects to the transverse ageostrophic circulations. It can be seen by comparing the T1 field (Fig. 7) to the total ageostrophic divergence field (Fig. 6) that only the divergence maxima D2 and D3 result from the pattern of the transverse ageostrophic component V_{an}. In particular there is no convergence on the cyclonic side of the entrance region of the jet streak JS2 (Fig. 6); there is instead a divergence maximum noted D1 induced by curvature effects. The midtropospheric vertical velocities in the entrance region of the jet streak JS2 are ascendant on both sides of the jet axis, as can be seen in Fig. 10. The direct vertical transverse circulation in the entrance region of the jet streak JS2, which could have been expected does not exist. So, this case study gives an example of flow pattern where curvature effects result in midtropospheric ascendant velocities below the cyclonic side of the entrance region of the jet streak, which inhibits the direct transverse ageostrophic circulation associated to the confluence mechanism. It is a complimentary case of flow pattern to that discussed by Keyser and Shapiro (1986); i.e., the case of the jet–front system located at the base of a long-wave trough, for which they suggest a favorable superposition of the upward

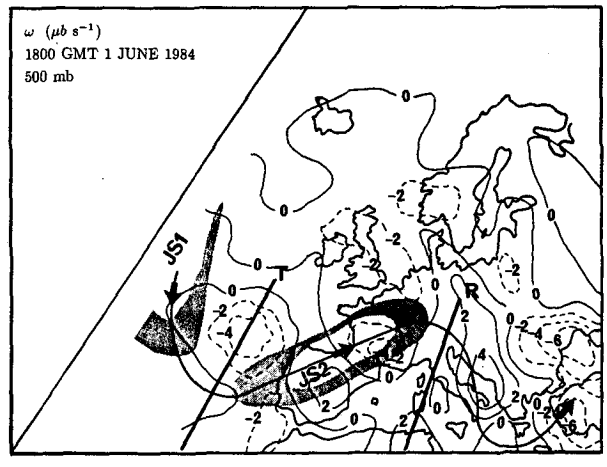

FIG. 10. Vertical velocity field in pressure coordinates at 500 mb for 1800 UTC 1 June 1984, positive values indicate descent (solid lines), negative values indicate ascent (dashed lines), units in $\mu b\ s^{-1}$. Key features as in Fig. 2b.

branches of the cross- and along-contour circulations beneath the jet axis.

The upper-tropospheric fields of the total ageostrophic divergence (Fig. 6), the transverse ageostrophic component (Fig. 5a) and its contribution to the divergence (Fig. 7) allow us to diagnose in the exit region of the jet streak JS2 an indirect transverse circulation. As can be seen in Fig. 11, which shows the component of the three-dimensional ageostrophic wind in the plane of the cross section along axis AB (see Fig. 2b), an indirect transverse circulation is actually observed in this region. Upward midtropospheric velocities of the order of -3.5 μb s^{-1} are observed below the maxima of divergence D3 on the cyclonic side of the jet axis (noted J on Fig. 11). In the upper troposphere the horizontal ageostrophic component in the plane of the cross section AB is of the order of 15 m s^{-1} within the jet core. Midtropospheric subsident velocities of the order of 1 μb s^{-1} are found on the anticyclonic side of the jet axis J, below the upper-level maximum of convergence induced by the term T1 in the exit region of the jet streak JS2 (Fig. 7). On the south extremity of the cross section AB, midtropospheric subsident motions are of the order of 4 to 5 μb s^{-1}. They are associated with the convergence maximum, noted C2 in the total ageostrophic divergence field (Fig. 6), induced by curvature effects.

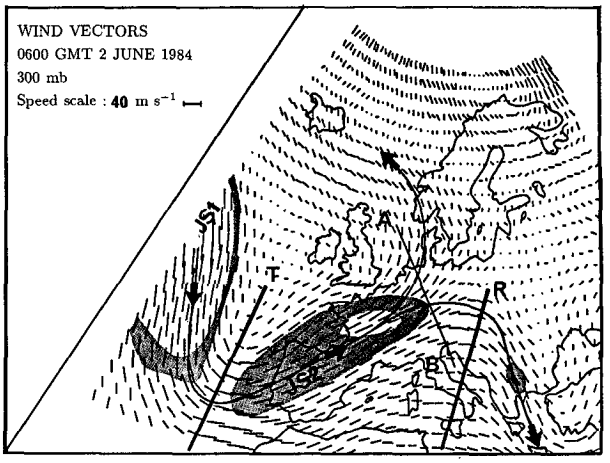

FIG. 12. Wind vectors at 300 mb for 0600 UTC 2 June 1984. Shading represents wind speed interval between 40 and 50 m s^{-1} to depict jet streaks indicated by JS1 and JS2. The line with arrows indicates the axis of highest wind speeds. The trough and ridge axis are noted T and R respectively.

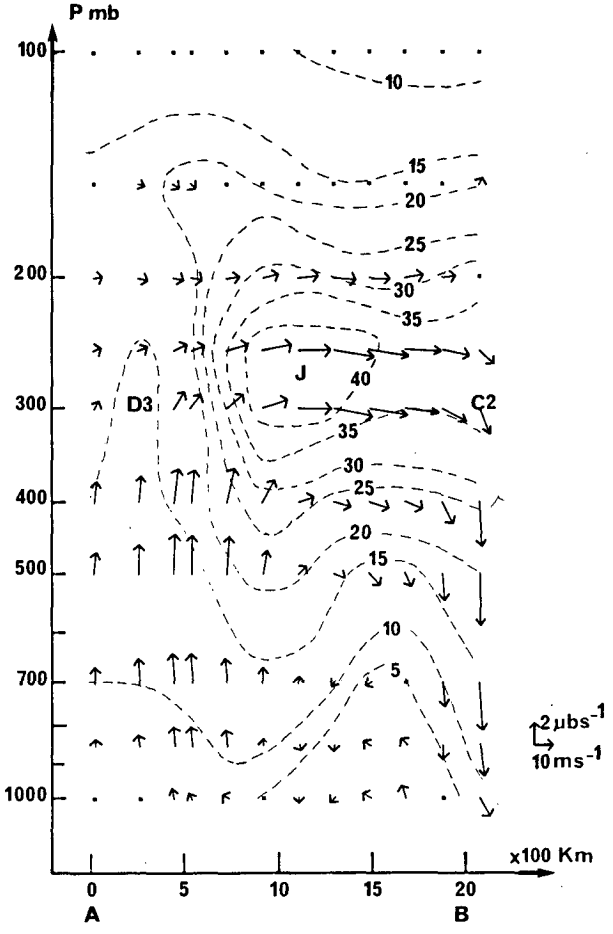

FIG. 11. Vector representation of vertical motions and ageostrophic wind components tangential to the plane of the cross section along axis AB shown in Fig. 2b (1800 UTC 1 June 1984), total wind isotachs in dashed lines, units in m s^{-1}, jet axis is indicated by J, maxima of convergence and divergence at 300 mb are indicated by D3 and C2 (see Fig. 6), magnitudes of ageostrophic wind and vertical velocity components are represented by vector scales on lower-right margin of the figure. Deduced from ECMWF data.

The natural component fields of the ageostrophic wind in the upper troposphere are then of great utility in interpreting the upper-tropospheric divergence field formation and in diagnosing ageostrophic circulations in the depth of the troposphere. The possibility to get these analyzed and predicted fields from numerical models on a routine basis as good as 6 hours allow investigations of the relationship between ageostrophic circulations associated with jet–front systems and circulations in the vicinity of lower tropospheric fronts.

In the next two sections, the analyses of the situations at 0600 UTC on 2 and 3 June 1984 show examples of an indirect ageostrophic circulation in a case of non-negligible curvature effects and in a case of warm advection respectively.

4. Case study on the 2 June 1984 0600 UTC

Figure 12 displays the wind vectors at 300 mb, 0600 UTC 2 June 1984. By comparing first the fields of the natural components V_{an} and V_{as} of the ageostrophic wind (Figs. 13 and 14), and second their respective contributions to the ageostrophic divergence field (Figs. 15 and 16), it can be seen that curvature effects in the entrance region of the jet streak JS2 are once more predominant. Consequently no signature of a direct

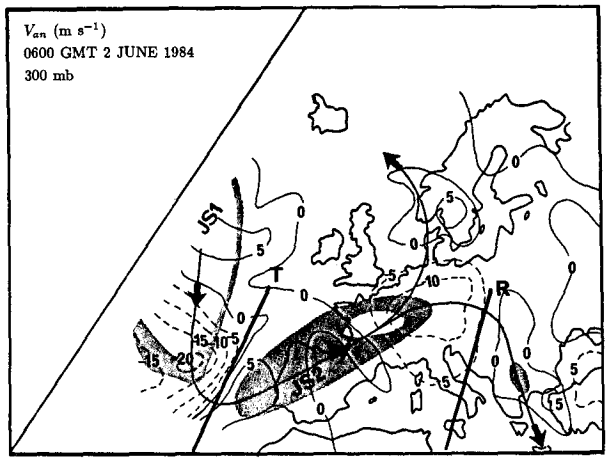

FIG. 13. Transverse ageostrophic wind component V_{an} at 300 mb for 0600 UTC 2 June 1984. Positive values in solid lines, negative values in dashed lines, units in m s^{-1}. Key features labeled as in Fig. 12.

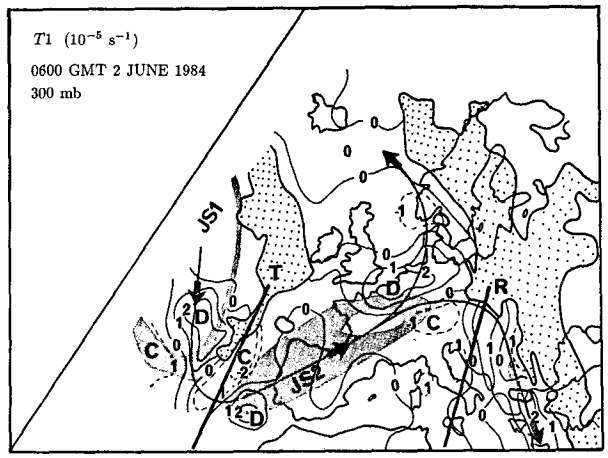

FIG. 15. Ageostrophic divergence field related to the term T1 (see text) at 300 mb for 0600 UTC 2 June 1984, positive values in solid lines, negative values in dashed lines, units ($\times 10^{-5}$ s^{-1}). Stippled regions are regions for which the quantity E (see text) is greater than 0.3×10^{-5} s^{-1}. Key features labeled as in Fig. 12.

transverse ageostrophic circulation in the upper-tropospheric ageostrophic divergence field (see Fig. 17) is observed in the entrance region of the jet streak JS2.

More generally as long as this flow pattern, i.e., the two jet streaks JS1 and JS2, respectively, upstream and downstream of the trough axis T, has maintained during the evolution of the baroclinic wave until the 3 June 1984, no direct transverse circulation has been observed in the entrance region of the jet streak JS2. This result is of particular interest because it shows an example of a flow in which the tropopause folding mechanism associated with the direct circulation (Uccellini et al. 1985; Keyser and Pecnick 1985a,b; Keyser and Shapiro 1986; Uccellini 1986) could not be initiated in the entrance region of the jet streak JS2.

In the exit region of the jet streak JS2 the diffluence of the flow is well pronounced (Fig. 12). The contributions of the natural components V_{an} and V_{as} of the ageostrophic wind to the divergence field (Figs. 15 and 16) are opposite in this region. However the contribution of the natural component V_{an} to the total ageostrophic divergence field (Fig. 17) is predominant: a signature of an indirect transverse ageostrophic circulation is detected in this last field. Figure 18 shows a projection of the three-dimensional component of the ageostrophic wind in the plane of the cross section AB (see Fig. 12) in the exit region of the jet streak JS2. An indirect transverse circulation is well defined in this vertical plane. The entire depth of the troposphere is

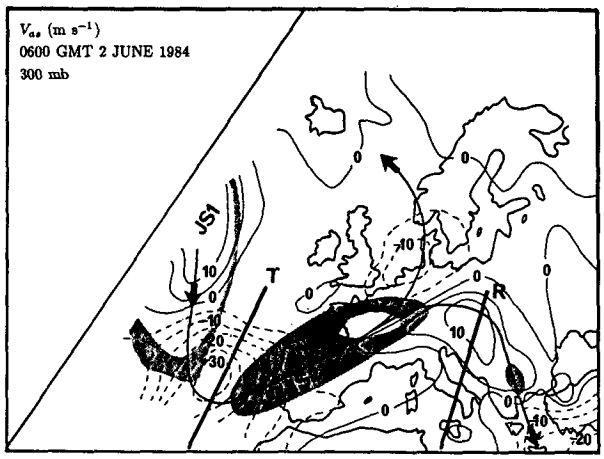

FIG. 14. Alongstream ageostrophic component V_{as}. Positive values in solid lines, negative values in dashed lines, units in m s^{-1}. Key features labeled as in Fig. 12.

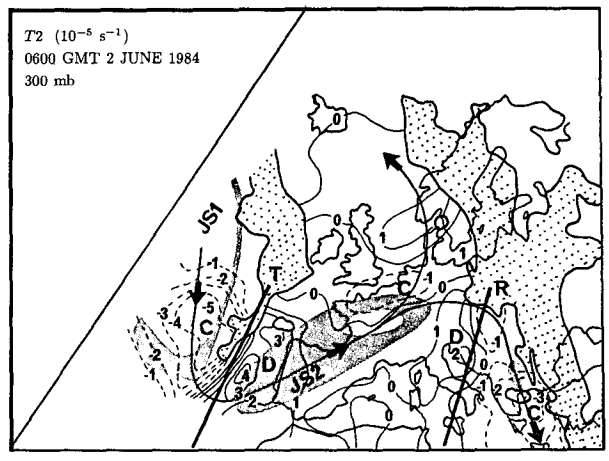

FIG. 16. Ageostrophic divergence field related to the term T2 (see text) at 300 mb for 0600 UTC 2 June 1984, positive values in solid lines, negative values in dashed lines, units ($\times 10^{-5}$ s^{-1}). Key features as in Fig. 12 and Fig. 15.

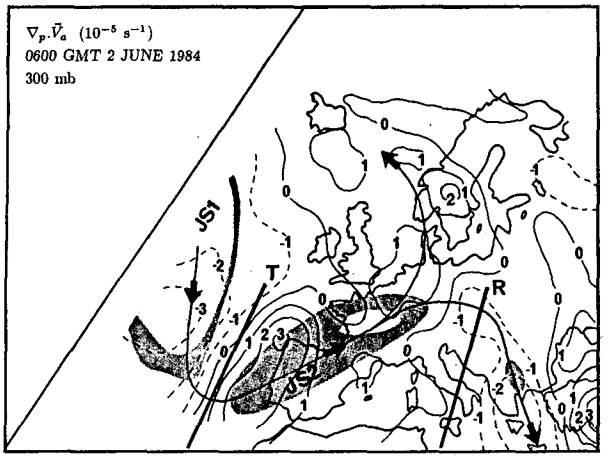

FIG. 17. Ageostrophic divergence field at 300 mb for 0600 UTC 2 June 1984; positive values in solid lines, negative values in dashed lines, units ($\times 10^{-5}$ s^{-1}). Key features as in Fig. 12 and Fig. 15.

affected by positive and negative vertical velocities of the order of $|2|$ μb s^{-1}, respectively, associated to the upward and downward branches of the indirect transverse circulation on each side of the jet axis.

5. Lateral shift of the transverse circulations and thermal advections

Among the cases studied during the period ranging from 1 to 3 June 1984, several exhibited a lateral shift of the upper-level transverse ageostrophic component, and sometimes of the transverse circulation itself, towards the anticyclonic side of the jet axis.

For the case of 1800 UTC 1 June 1984, which is presented in section 3 of this paper, such a lateral shift of the transverse component is observed in the entrance region of the jet streak JS2 as can be seen on Fig. 5a, and also on Fig. 7 through its contribution to the total divergence. However it has been shown that curvature effects in the entrance region of the jet streak JS2 at 1800 UTC 1 June 1984 are predominant so as to inhibit the midtropospheric vertical motions associated to the direct circulation expected in this region. The case study of 0600 UTC 3 June 1984 is more meaningful concerning a lateral shift of a transverse circulation.

Figure 19 shows the geopotential and temperature fields in the upper troposphere at 0600 UTC 3 June 1984. In the exit region of the jet streak JS2 (see Figs. 19 and 20) the flow is relatively straight, so the effects of curvature of the trajectories are not significant. One can observe on Fig. 20 a weak maximum of the order of -5 to -10 m s^{-1} of the transverse ageostrophic component V_{an} which is shifted laterally on the anticyclonic side of the exit region of the jet streak JS2 at a distance of about 300 km. Patterns of the divergence field of the ageostrophic wind (Fig. 21) complement the signature of an indirect and laterally shifted ageostrophic circulation in the exit region of this jet streak. Positive values of divergence are found on the west side of the maximum of V_{an} nearby the jet axis, whereas a maximum of convergence is found on the anticyclonic side of the jet axis on the east side of the maximum V_{an}.

In order to show the indirect transverse circulation in the exit region of the jet streak JS2, a projection of the three-dimensional component of the ageostrophic wind is made in the plane of the cross section AB (see Fig. 20) and is displayed on the Fig. 22. This figure shows an indirect transverse ageostrophic circulation, laterally shifted on the anticyclonic side of the jet axis of about 300 km. The upward branch of this circulation is located beneath the jet axis with midtropospheric vertical velocities of the order of -4 μb s^{-1}, whereas its downward branch shifted on the anticyclonic side of the jet axis displays midtropospheric vertical velocities of the order of 2 μb s^{-1}. In the lower troposphere,

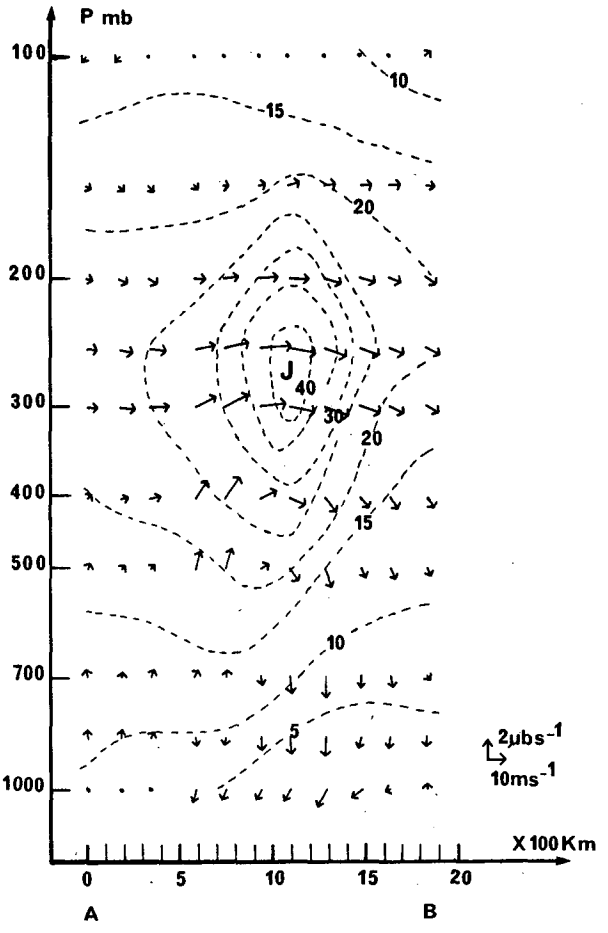

FIG. 18. Vector representation of vertical motions and ageostrophic wind components tangential to the plane of the cross section along axis AB in Fig. 12 (0600 UTC 2 June 1984), total wind isotachs in dashed lines, units in m s^{-1}, jet axis is indicated by J, magnitudes of ageostrophic wind and vertical velocity components are represented by vector scales on lower-right margin of the figure. Deduced from ECMWF data.

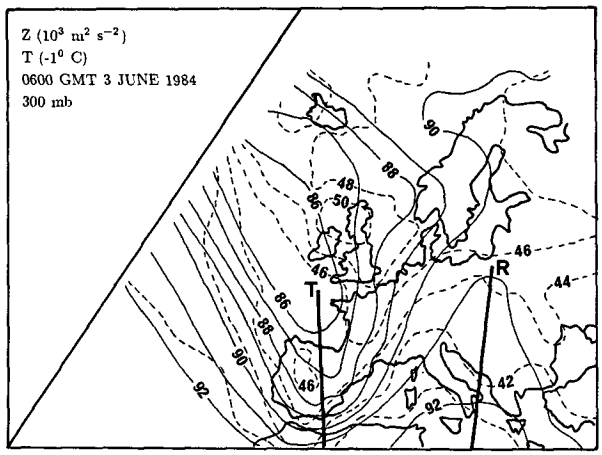

FIG. 19. Geopotential and temperature fields at 300 mb for 0600 UTC 3 June 1984, geopotential contours are drawn in solid lines ($\times 10^3$ m^2 s^{-2}), isotherms in dashed lines (°C). The trough and ridge axis are noted T and R respectively.

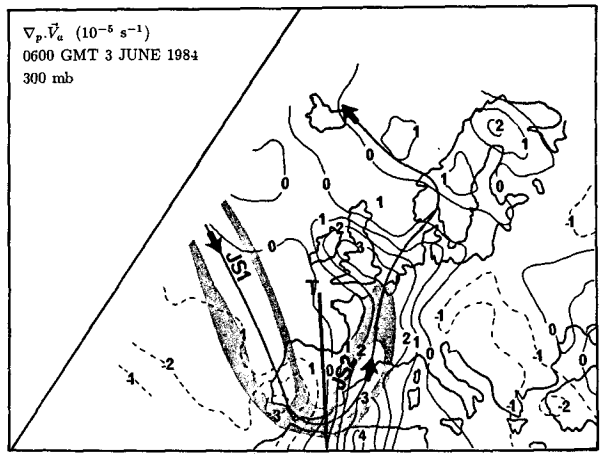

FIG. 21. Ageostrophic divergence field at 300 mb for 0600 UTC 3 June 1984; positive values in solid lines, negative values in dashed lines, units ($\times 10^{-5}$ s^{-1}). Key features labeled as in Fig. 20.

about the 850 mb level, horizontal ageostrophic velocities about 4 m s^{-1} complement the indirect circulation.

The case study of 0600 UTC 3 June 1984 shows that the structure of the upper-level wind field is such that the mass adjustment induced by speed changes is not symetrical to the jet axis, i.e., the axis of the highest wind speeds. The approach based on the concept of mass adjustment and computations of the mass divergence profiles (Uccellini and Johnson 1979), or the approach used in this paper are based on the structure of the wind field and they can diagnose an eventual lateral shift of the transverse circulation. Bjerknes (1951) discusses the shift of the transverse circulation

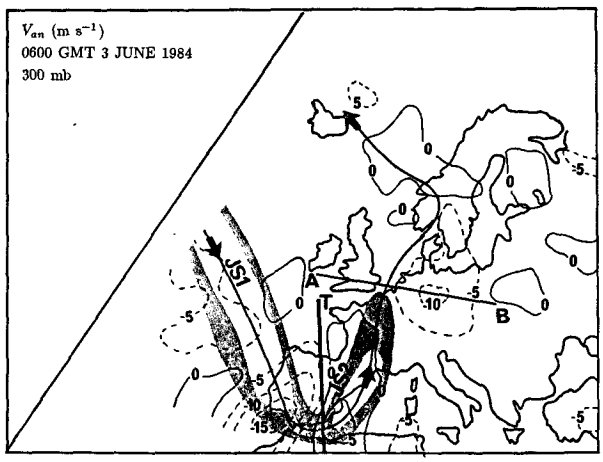

FIG. 20. Transverse ageostrophic wind component V_{an} at 300 mb for 0600 UTC 3 June 1984. Positive values in solid lines, negative values in dashed lines, units in m s^{-1}. Shading represents wind speed interval between 40 and 50 m s^{-1} to depict jet streaks indicated by JS1 and JS2. The line with arrows indicates the axis of highest wind speeds. AB indicates the plane of the cross-section of Fig. 22.

to the anticyclonic side of the jet as a function of reduced hydrodynamic stability. Uccellini et al. (1984) argue that such a shift could be related to smaller values of absolute vorticity associated to the anticyclonic shear and curvature within the jet streak. Though of course, the "information" of lateral shift is implicitly contained in the structure of the upper-level wind field, it seems difficult to extract it from a quick look on the isotachs fields that are commonly available to the forecasters. From a nowcasting point of view it would be very useful to have a criterion which allows the forecasters to know if the transverse circulations are centered about the jet axis or are laterally shifted towards the anticyclonic or cyclonic side of the jet axis.

Apart from the curvature effects, other authors have also discussed the lateral shift of the transverse circulations with a frontogenetic approach. Shapiro (1981) and Keyser and Pecnick (1985a,b) have shown through simulations on idealized flows that the shift of the transverse circulations could be related to an horizontal shear forcing that adds, if a thermal advection exists, to the geostrophic confluence (diffluence) forcing in the entrance (exit) region of the jet. Conceptual schematics of the lateral shifts of the transverse circulations have been reviewed by Keyser and Shapiro (1986) with deductions based on the Sawyer–Eliassen equation. Uccellini et al. (1985) and Uccellini (1986) have related their findings of a tropopause fold event induced by a strong subsidence on the warm side of the front with the lateral shift of the direct circulation on the anticyclonic side of the jet entrance placed in a region where a cold advection coincides with a cyclonic geostrophic wind shear.

In our case studies the thermal advection in the exit region of the jet streak JS2 at 0600 UTC 3 June 1984 is positive (see Fig. 19 and 20), and a lateral shift of the indirect circulation is actually observed towards

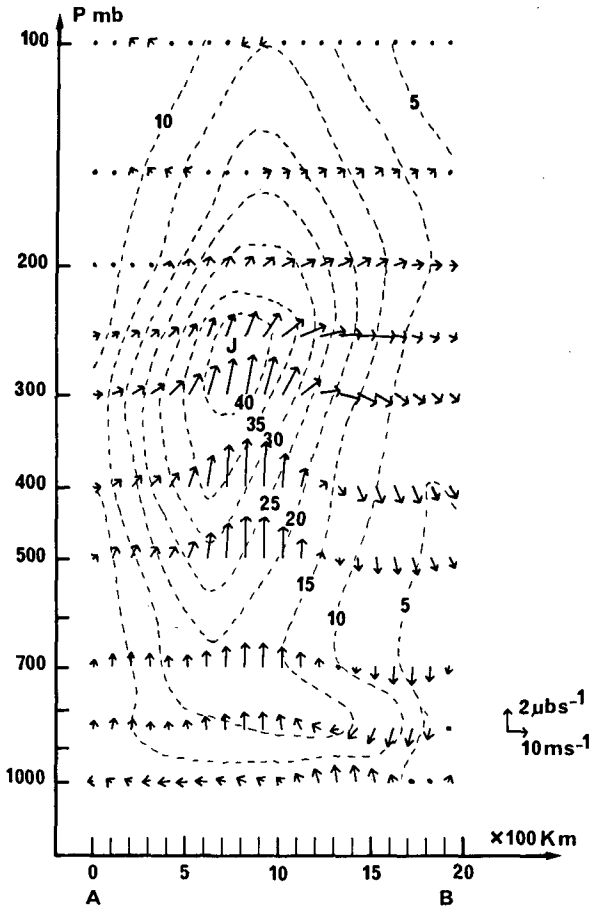

FIG. 22. Vector representation of vertical motions and ageostrophic wind components tangential to the plane of the cross section along axis AB shown in Fig. 20 (0600 UTC 3 June 1984), total wind isotachs in dashed lines, units in m s^{-1}, jet axis is indicated by J, magnitudes of ageostrophic wind and vertical velocity components are represented by vector scales on lower-right margin of the figure. Deduced from ECMWF data.

the anticyclonic side of the jet axis (Fig. 20), in agreement with the previous numerical and conceptual studies. Furthermore, the lateral shift of the indirect circulation towards the anticyclonic side of the jet axis has continued during the five consecutive analysis fields from 0000 UTC 3 June 1984 to 0000 UTC 4 June 1984, i.e., the period for which the thermal wave leads the height wave (not shown). In the same way at 1800 UTC 1 June 1984, the negative thermal advection in the entrance region of the jet streak JS2 (Fig. 2a,b) and the lateral shift of the transverse component (Fig. 5a) appear to corroborate the previous studies.

The two case studies described in this section are obviously not documented enough to authorize a straightforward generalization; in particular the ECMWF data, which this study is based on, are not appropriate to solve at the desired scales the features of upper-level frontal zones and tropopause folds (Elsberry and Kirchoffer 1988). Other well-documented case studies are certainly needed, using appropriate mesoscale models.

6. Conclusion

We have analyzed the contributions to the divergence field of the transverse (cross-stream) and the alongstream components of the ageostrophic wind in upper-tropospheric jet–front systems taking advantage of the regular gridded form, the dynamical consistency, and the spatial resolution of datasets of ECMWF model analyses to work in the natural coordinate system.

The role of the alongstream wind variations in forcing transverse direct and indirect ageostrophic circulations in the entrance and exit region of straight jet streaks respectively (Bjerknes 1951; Uccellini and Johnson 1979) have thus been investigated in several observed flow patterns. The contribution of the alongstream component of the ageostrophic wind to the upper-tropospheric divergence field has been analyzed in order to show the three-dimensional modifications introduced by curvature effects on the transverse circulations.

Alongstream curvature advection is shown to be the predominant term concerning the contribution of curvature effects to the upper-tropospheric divergence wind field in this case study. It results in vertical ascendant (subsident) midtropospheric motions downstream (upstream) of the trough axis of the baroclinic wave. It has been shown, for the entrance region of a jet–front system located downstream of the trough axis in the present case study, that curvature effects can be predominant to such a point that the signature of the direct transverse ageostrophic circulation do not appear in the upper-tropospheric divergence field and therefore in the midtropospheric vertical velocity field nearby the jet–front system.

In a case of a jet–front system located at the base of a long-wave trough, Keyser and Shapiro (1986), taking into account both the forcing mechanisms of the transverse circulations and the curvature effects, suggest a favorable superposition of the upward branches of the transverse and alongstream circulations beneath the jet axis. In our case study the three-dimensional modifications induced by curvature effects on transverse ageostrophic circulations yield a flow pattern different from the above study; the composition of transverse and alongstream ageostrophic components do not lead to such a favorable superposition.

For several situations of a jet–front system embedded in an evolving baroclinic wave, an indirect transverse circulation has been identified in the jet-streak exit region for which vertical velocities within the upward and downward tropospheric branches located on each side of the jet axis are of the order of 2 to 4 $\mu b\ s^{-1}$. For a case of warm advection in the exit region of a jet streak, an indirect transverse circulation has been

found laterally shifted on the anticyclonic side of the jet axis on a distance about 300 km. This result could be an illustration of the effect of the horizontal shear forcing in case of thermal advection, as has been shown by Keyser and Pecnick (1985a,b) from numerical results on idealized flows, reviewed by Keyser and Shapiro (1986), and analyzed on case studies by Uccellini et al. (1985) and Uccellini (1986). Further well documented case studies are certainly needed in order to valid such an interpretation of the lateral shift of the transverse circulation.

We have shown that there is no noteworthy bias introduced by the ECMWF analysis procedure on the retrieved ageostrophic wind fields. So their direct use for diagnostic studies of ageostrophic circulations in jet–front systems appears more appropriate than the use of those derived from the quasi-geostrophic or the geostrophic momentum approximations. Using the natural coordinate system, we have shown that the examination on the constant pressure surface 300 mb of ageostrophic fields, as those of the natural components of the ageostrophic wind and those of the contribution of these components to the divergence wind, allow to infer in the entire depth of the troposphere the ageostrophic circulations associated to jet–front systems. It is hoped that the method of diagnostic analysis developed in this study will be useful to investigate the relationship between ageostrophic circulations in upper-tropospheric jet–front systems and circulations in the vicinity of lower tropospheric fronts.

Acknowledgments. The authors would like to thank the European Centre for Medium-Range Weather Forecasts for providing the numerical analysis used in this study. We have appreciated the useful comments of the reviewers, one of them is Dr L. W. Uccellini, they have helped us to clarify many crucial points of this study. We would like to thank them for the substantial time and effort they have contributed. We wish to acknowledge and express our gratitude to Yves Pointin for his suggestions during the development of this study. An acknowledgment is also extended to Jacqueline Duron and Robert Pejoux for their important technical support, and to Jeanne Squarise for the final correction of the paper.

REFERENCES

Achtor, T. H., and L. H. Horn, 1986: Spring season Colorado cyclones. Part I: Use of composites to relate upper and lower tropospheric wind fields. *J. Climate Appl. Meteor.*, **25,** 732–743.

Bjerknes, J., 1951: Extratropical cyclones. *Compendium of Meteorology,* T. F. Malone, Ed., Amer. Meteor. Soc., 577–598.

——, and J. Holmboe, 1944: On the theory of cyclones. *J. Meteor.*, **1,** 1–22.

Bluestein, H. B., and K. W. Thomas, 1984: Diagnosis of a jet streak in the vicinity of a severe weather outbreak in the Texas Panhandle. *Mon. Wea. Rev.*, **96,** 2501–2522.

Brill, K. F., L. W. Uccellini, R. P. Burkhart, T. T. Warner and R. A. Anthes, 1985: Numerical simulations of a transverse indirect circulation and low-level jet in the exit region of an upper-level jet. *J. Atmos. Sci.*, **42,** 962–988.

Buzzi, A., T. Nanni and M. Tagliazucca, 1977: Mid-tropospheric frontal zones: Numerical experiments with an isentropic coordinate primitive equation model. *Arch. Meteor. Geophys. Bioklim.*, **A26,** 155–178.

Cahir, J. J., 1971: Implications of circulations in the vicinity of jet streaks at subsynoptic scales. Ph.D. thesis, Pennsylvania State University, 170 pp.

Danielsen, E. F., 1959: The laminar structure of the atmosphere and its relation to the concept of tropopause. *Arch. Meteor. Geophys. Bioklim.*, **3,** 293–332.

——, 1968: Stratospheric-tropospheric exchange based on radioactivity, ozone, and potential vorticity. *J. Atmos. Sci.*, **25,** 502–518.

——, 1974: The relationship between severe weather, major dust storms and rapid large-scale cyclogenesis (I). Subsynoptic Extratropical Weather Systems: Observations, Analysis, Modeling and Prediction (Vol. II), National Center for Atmospheric Research, Boulder, CO, 215–225.

Eliassen, A., 1948: The quasi-static equations of motions. *Geofys. Publ.*, **17**(3), 1–44.

——, 1962: On the vertical circulation in frontal zones. *Geofys. Publ.*, **24,** 147–160.

Elsberry, R. L., and P. J. Kirchoffer, 1988: Upper-level forcing of explosive cyclogenesis over the ocean based on operationally analysed fields. *Wea. Forecasting,* **3,** 205–216.

Hoskins, B. J., M. E. McIntyre and A. W. Robertson, 1985: On the use and significance of isentropic potential vorticity maps. *Quart. J. Roy. Meteor. Soc.*, **111,** 877–946.

Keyser, D., 1985b: Part II: Diagnosis of ageostrophic circulations in a two-dimensional primitive equation model of frontogenesis. *J. Atmos. Sci.*, **42,** 1283–1305.

——, and M. J. Pecnick, 1985a: Part I: A two-dimensional primitive equation model of frontogenesis forced by confluence and horizontal shear. *J. Atmos. Sci.*, **42,** 1259–1282.

——, and M. A. Shapiro, 1986: A review of the structure and dynamics of upper-level frontal zones. *Mon. Wea. Rev.*, **114,** 452–499.

Lonnberg, P., and D. Shaw, 1986: ECMWF data assimilation. Scientific documentation. Research manual 1. ECMWF Research Department.

Lorenc, A. C., 1981: A global three-dimensional multivariate statistical interpolation scheme. *Mon. Wea. Rev.*, **109,** 701–721.

Meteorological Bulletin of ECMWF, 1982: Retrieval utility for ECMWF data-bank for reports and fields on standard pressure levels (GETDATA).

Murray, R., and S. M. Daniels, 1953: Transverse flow at entrance and exit to jet stream. *Quart. J. Roy. Meteor. Soc.*, **79,** 236–241.

Namias, J., and P. F. Clapp, 1949: Confluence theory of the high tropospheric jet stream. *J. Meteor.*, **6,** 330–336.

Newton, C. W., 1984b: Clinogenesis and frontogenesis in jet-stream waves. Part II: Channel model numerical experiments. *J. Atmos. Sci.*, **41,** 2735–2755.

——, and A. Trevisan, 1984a: Clinogenesis and frontogenesis in jet-stream waves. Part I: Analytical relations to wave structure. *J. Atmos. Sci.*, **41,** 2717–2734.

Palmen, E., and C. W. Newton, 1969: Atmospheric circulation systems. *Academic Press,* New York, 603 pp.

Reiter, E. R., 1961: *Jet-Stream Meteorology.* University of Chicago Press, 515 pp.

——, 1969: Tropopause circulations and jet streams. Climate of the free atmosphere. D. F. Rex, Ed., Publ. Vol. 4. *World Survey of Climatology,* 85–193.

——, 1975: Stratospheric-Tropospheric exchanges processes. *Rev. Geophys. Space Phys.*, **13,** 459–474.

Riehl, H., J. Badner, J. E., Hovde, N. E. Laseur, L. L. Means, W. C. Palmer, M. J. Schroeder, L. W. Snellman and others, 1952: *Forecasting in Middle Latitudes. Meteor. Monogr.*, No. 5, Amer. Meteor. Soc., 80 pp.

Sawyer, J. S., 1956: The vertical circulation at meteorological fronts

and its relation to frontogenesis. *Proc. Roy. Soc. London,* **A234,** 346–362.

Shapiro, M. A., 1980: Turbulent mixing within tropopause folds as a mechanism for the exchange of chemical constituents between the stratosphere and troposphere. *J. Atmos. Sci.,* **37,** 994–1004.

——, 1981: Frontogenesis and geostrophically forced secondary circulations in the vicinity of jet stream–frontal zone systems. *J. Atmos. Sci.,* **38,** 954–973.

——, 1982: Mesoscale Weather systems of the Central United States. Cooperative Institute of Research in Environmental Sciences, University of Colorado/NOAA, Boulder, CO, 78 pp.

——, 1983: Mesoscale Weather systems of the Central United States. The National STORM Program: Scientific and Technological Bases and Major Objectives, [University Corporation for Atmospheric Research, P.O. Box 3000, Boulder, CO, 80307].

——, and P. J. Kennedy, 1981: Research aircraft measurements of jet stream geostrophic and ageostrophic winds. *J. Atmos. Sci.,* **38,** 2642–2652.

Staley, D. O., 1960: Evaluation of the potential vorticity changes near the tropopause and the related vertical motions, vertical advections of vorticity, and transfer of radioactives debris from stratosphere to troposphere. *J. Meteor.,* **17**(6), 591–620.

Uccellini, L. W., 1986: The possible influence of upstream upper-level baroclinic processes on the development of the *QE II* storm. *Mon. Wea. Rev.,* **114,** 1019–1027.

——, and D. R. Johnson, 1979: The coupling of upper and lower tropospheric jet streaks and implications for the development of severe convective storms. *Mon. Wea. Rev.,* **107,** 682–703.

——, P. J. Kocin, R. A. Petersen, C. H. Wash and K. F. Brill, 1984: The Presidents' Day cyclone of 18–19 February 1979. Synoptic overview and analysis of the subtropical jet streak influencing the pre-cyclogenetic period. *Mon. Wea. Rev.,* **112,** 31–55.

——, D. Keyser, K. F. Brill and C. H. Wash, 1985: The Presidents' Day cyclone of 18–19 February 1979: Influence of upstream trough amplification and associated tropopause folding on rapid cyclogenesis. *Mon. Wea. Rev.,* **113,** 962–988.

——, and P. J. Kocin, 1987: The interaction of jet streak circulations during heavy snow events along the east coast of the United States. *Wea. Forecasting,* **1,** 289–308.

——, R. A. Petersen, K. F. Brill, P. J. Kocin and J. T. Tuccillo, 1987: Synergistic interactions between an upper-level jet streak and diabatic processes that influence the development of a low-level jet and secondary coastal cyclone. *Mon. Wea. Rev.,* **115,** 2227–2261.